Substructure Interface Reduction with Iwan Elements to Capture Nonlinearity

Aabhas Singh

University of Wisconsin – Madison

singh36@wisc.edu

Matthew S. Allen

University of Wisconsin – Madison

msallen@engr.wisc.edu

Robert J. Kuether

Sandia National Laboratories

rjkueth@sandia.gov

ABSTRACT

In structural dynamics, finite element models for structures with bolted interfaces typically use multi-point constraints (MPC) and/or spring element(s) to join contact interfaces. Some prior works have used RBE3 averaging MPCs or rigid bar MPCs to reduce the contact interface, and then Iwan joints were added to capture the nonlinear behavior. When doing this, a physical Iwan element is needed for each joint or connection in the assembly, so if there are many joints then there is a large set of unknown joint parameters that need to be calibrated when updating the FEM. This work presents an alternate approach where the contact interface is reduced using modes that allow some flexibility of the interface, so each bolted joint does not need to be considered separately. Specifically, system-level characteristic constraint (S-CC) modes and Coppolino's augmented Guyan reduction method are used to reduce the contact interface to a small number of shapes, which describe how the interface deforms. Then, a four-parameter Iwan element can be applied to the S-CC DOF to capture the joint nonlinearity. Ideally a small number of Iwan elements is needed so there are relatively few unknown parameters to identify when calibrating the model, while still potentially capturing coupling between the modes. The methodology is demonstrated on the "S4 Beam" benchmark structure to evaluate the accuracy of the method and ability to capture the coupling in the nonlinear response of the modes.

Keywords: Iwan Elements, Joints, Quasi-Static Modal Analysis, Reduction Techniques, Interface Reduction, Hurty/Craig-Bampton Reduction, Hysteresis

1. INTRODUCTION

Even with the growing presence of additive manufacturing in industry, it is difficult to manufacture large structures without the use of sub-assemblies, and hence interfaces or joints between the parts. Finite element software can be used to predict structural responses in these structures, but significant challenges arise when trying to capture the effects of frictional contact of the joints due to the small length scales of the physics. It is common to observe energy dissipation due to the presence of joints, and hence a change in the effective modal damping (and also the natural frequencies) as a function of vibration amplitude for weakly nonlinear systems. If the slip in the joints is large enough, complicated phenomena such as multi-harmonic responses, modal coupling, and even catastrophic failure can be observed.

Existing finite element software can solve contact problems with friction [1], but the mesh must be refined near the interface in order to obtain a predictive model. When a model contains many joints, the

high-resolution FEM becomes highly infeasible. This was illustrated recently by Jewel et. al [2] who demonstrated that when the mesh was adequately refined and the solver was tuned to accurately solve the contact mechanics problem, tens of hours were required to obtain accurate solutions for the static response of a structure with fewer than three joints. It would be computationally expensive to perform dynamic simulations with such a model, and even more so for realistic structures with hundreds of joints. As a result, the majority of dynamic models use some sort of multi-point constraint (MPCs) and/or spring elements to tie together nodes near the contact interface to generate the so-called whole joint model with six independent degrees-of-freedom. Linear springs or multi-parameter nonlinear elements are placed at these nodes to approximate the physics within the joint to capture amplitude dependency of the frequency and damping of a vibration mode. These springs/constraints are meant to approximate the actual contact, where in reality there are certain regions in the interface that have adequate pressure to remain fully in contact (i.e. stuck). In other regions, the material may have no contact stiffness due to gapping or may switch between opened and closed constraints as the structure vibrates.

The parameters for a whole-joint model, such as an Iwan element [3] to model shear in lap joints, cannot currently be predicted from first principles, so measurements and model updating are used to calibrate the joint parameters until the model reproduces the measured response. The recently developed Quasi-Static Modal Analysis (QSMA) approach [4],[5] can be used determine the amplitude dependency of the modes of a finite element model and iteratively update the parameters. Lacayo et al. [5] demonstrated this workflow to update a reduced model of the Brake-Reuss (BRB) beam. Singh et. al. further explored this in [6], showing how the nonlinear results vary based on the decisions used to create the MPCs of the interface. The S4 Beam structure studied at Sandia National Laboratories Nonlinear Mechanics and Dynamics Institute in 2017 is shown in Figure 1 [7] and previous research by Singh, Allen, and Kuether studied the influence of the spidering method on the model updating process. They found that different results may be obtained during nonlinear model updating depending on whether the spiders were rigid (i.e. Rigid Bar) or averaging type (i.e. RBE3). Additionally, the results depend on the contact area over which the spiders were connected. In the full contact interface with the stiffer constraint, the model could fit the measurements very well, while in the reduced interface to the contact area and the averaging MPC, a Pareto front was observed as seen by Lacayo [5].

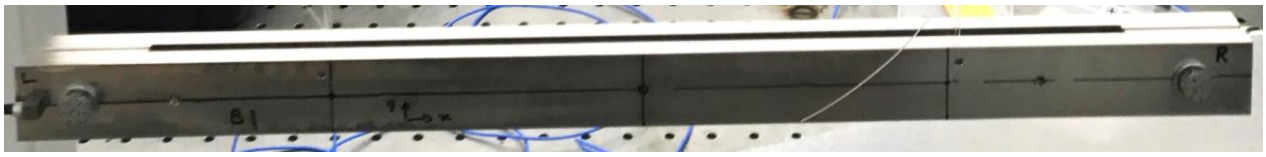

Figure 1: The S4 Beam side view

To counter the limitations observed in prior studies, this work seeks to develop a methodology that allows a transition from the traditional spidering approach to a continuous interface modeled in detail in FEM. We present an approach that retains some flexibility in the interface, while still connecting the subcomponents with a few Iwan joints. To do so, different reduction techniques are presented and applied to the S4 Beam. First, the beams are reduced to the interface through a Hurty/Craig Bampton reduction, to minimize the size of the model. Then a preload is applied using the penalty stiffness method as shown by Hughes et. al. [8]. Finally, the preloaded model is reduced using a System Level Characteristic Constraint Reduction [9] and truncated to match the linear frequencies of the Hurty/Craig Bampton (HCB) model. An additional reduction method, Coppolino's generalized Guyan reduction [10], is evaluated to calibrate linear frequencies and is shown in the Appendix.

Once the linearized reduced models are created, modal Iwan elements are appended to the linear stiffness terms in the ROM, as described in the following sections, and QSMA is used to compute the amplitude dependent damping and frequency. This work presents a proof of concept showing the effectiveness of the S-CC reduction technique to reproduce the expected behavior of each mode of the assembled structure. This allows for coupling at the vibration mode level by adding in decoupled Iwan

elements at the S-CC level. Furthermore, it begins to address the concern of the variation in results with the spidered models, by reducing the model to a set of DOF in the modal domain while maintaining the flexibility of the interface (no rigid or averaging constraints).

2. THEORY

2.1 Hurty/Craig Bampton Reduction and Model Preload

Finite element models quickly become computationally expensive and element-dense when incorporating the detail around joints (i.e. rivets, bolted joints, mechanisms, etc…). To reduce this computational burden, reduced order models (ROMs) are used to approximate the full-order model at a set of reduction nodes near the mechanical interfaces. The approximation requires that these components remain linear and that the only source of nonlinearity within in the joined system is at the contact interface [11]. Although many methods of model reduction exist, this paper will focus on the HCB method as discussed in [12]. The FE discretized equations of motion for an undamped multi-degree of freedom (MDOF) system are given by Eq. 1, where $\mathbf{M}$ is the mass matrix, $\mathbf{K}$ is the stiffness matrix, $\mathbf{F}$ is the external forcing, $\mathbf{F}_J(\mathbf{u})$ is the joint force from the preload analysis, $\mathbf{u}$ is the physical displacement, and $\ddot{\mathbf{u}}$ is the physical acceleration.

$$\mathbf{M}\ddot{\mathbf{u}} + \mathbf{K}\mathbf{u} + \mathbf{F}_\mathbf{J}(\mathbf{u}) = \mathbf{F} \tag{1}$$

The system can be equivalently written with matrices partitioned between the boundary and internal DOFs as

$$\begin{bmatrix}\mathbf{M}_{\mathrm{ii}} & \mathbf{M}_{\mathrm{ib}}\\ \mathbf{M}_{\mathrm{bi}} & \mathbf{M}_{\mathrm{bb}}\end{bmatrix}\begin{Bmatrix}\ddot{\mathbf{u}}_{\mathrm{i}}\\ \ddot{\mathbf{u}}_{\mathrm{b}}\end{Bmatrix} + \begin{bmatrix}\mathbf{K}_{\mathrm{ii}} & \mathbf{K}_{\mathrm{ib}}\\ \mathbf{K}_{\mathrm{bi}} & \mathbf{K}_{\mathrm{bb}}\end{bmatrix}\begin{Bmatrix}\mathbf{u}_{\mathrm{i}}\\ \mathbf{u}_{\mathrm{b}}\end{Bmatrix} + \begin{Bmatrix}0\\ \mathbf{F}_{\mathrm{J,b}}(\mathbf{u}_{\mathrm{b}})\end{Bmatrix} = \begin{Bmatrix}0\\ \mathbf{F}_{\mathrm{b}}\end{Bmatrix} \tag{2}$$

where subscripts *b* and *i* represent the boundary and interior DOF respectively. Note that only the boundary DOF are assumed to be forced either externally or internally through the joint. Then, a small number of fixed interface modes[1], $\mathbf{\Phi}$, are computed and that basis is augmented with constraint modes[2], $\mathbf{\Psi}$, as detailed [13], to obtain the HCB transformation matrix in Eq. 3.

$$\begin{Bmatrix}\mathbf{u}_{\mathrm{i}}\\ \mathbf{u}_{\mathrm{b}}\end{Bmatrix} = \mathbf{T}^{\mathrm{HCB}}\begin{Bmatrix}\mathbf{q}_{\mathrm{i}}\\ \mathbf{u}_{\mathrm{b}}\end{Bmatrix} = \begin{bmatrix}\mathbf{\Phi} & \mathbf{\Psi}\\ \mathbf{0} & \mathbf{I}\end{bmatrix}\begin{Bmatrix}\mathbf{q}_{\mathrm{i}}\\ \mathbf{u}_{\mathrm{b}}\end{Bmatrix} \tag{3}$$

This transformation then reduces the equations of motion to those shown in Eq. 4.

$$(\mathbf{T}^{\mathrm{HCB}})^{\mathrm{T}}\begin{bmatrix}\mathbf{M}_{\mathrm{ii}} & \mathbf{M}_{\mathrm{ib}}\\ \mathbf{M}_{\mathrm{bi}} & \mathbf{M}_{\mathrm{bb}}\end{bmatrix}\mathbf{T}^{\mathrm{HCB}}\begin{Bmatrix}\ddot{\mathbf{q}}_{\mathrm{i}}\\ \ddot{\mathbf{u}}_{\mathrm{b}}\end{Bmatrix} + (\mathbf{T}^{\mathrm{HCB}})^{\mathrm{T}}\begin{bmatrix}\mathbf{K}_{\mathrm{ii}} & \mathbf{K}_{\mathrm{ib}}\\ \mathbf{K}_{\mathrm{bi}} & \mathbf{K}_{\mathrm{bb}}\end{bmatrix}\mathbf{T}^{\mathrm{HCB}}\begin{Bmatrix}\mathbf{q}_{\mathrm{i}}\\ \mathbf{u}_{\mathrm{b}}\end{Bmatrix} + (\mathbf{T}^{\mathrm{HCB}})^{\mathrm{T}}\begin{Bmatrix}\mathbf{0}\\ \mathbf{F}_{\mathrm{J,b}}(\mathbf{u}_{\mathrm{b}})\end{Bmatrix} = (\mathbf{T}^{\mathrm{HCB}})^{\mathrm{T}}\begin{Bmatrix}\mathbf{0}\\ \mathbf{F}_{\mathrm{b}}\end{Bmatrix} \tag{4}$$

which in compact form becomes,

$$\begin{bmatrix}\mathbf{I} & \bar{\mathbf{M}}_{\mathbf{ib}}\\ \bar{\mathbf{M}}_{\mathbf{bi}} & \bar{\mathbf{M}}_{\mathbf{bb}}\end{bmatrix}\begin{Bmatrix}\ddot{\mathbf{q}}_{\mathrm{i}}\\ \ddot{\mathbf{u}}_{\mathrm{b}}\end{Bmatrix} + \begin{bmatrix}\mathbf{\Lambda}_{\mathbf{ii}} & \mathbf{0}\\ \mathbf{0} & \bar{\mathbf{K}}_{\mathbf{bb}}\end{bmatrix}\begin{Bmatrix}\mathbf{q}_{\mathrm{i}}\\ \mathbf{u}_{\mathrm{b}}\end{Bmatrix} + \begin{Bmatrix}\mathbf{0}\\ \mathbf{F}_{\mathrm{J,b}}(\mathbf{u}_{\mathrm{b}})\end{Bmatrix} = \begin{Bmatrix}\mathbf{0}\\ \mathbf{F}_{\mathrm{b}}\end{Bmatrix} \tag{5}$$

The ROM can be used to analyze the dynamic response of a structure more efficiently than the full finite element model, depending on the number of boundary DOF needed to retain the nonlinear internal force vector. The quasi-static HCB model is solved for the preloaded equilibrium state as,

[1] Fixed interface modes are normal modes obtained by fixing the interface between two subcomponents

[2] Constraint modes are obtained by deflecting a single interface DOF by a unit displacement while fixing the other DOF

$$\begin{bmatrix} \boldsymbol{\Lambda}_{\mathbf{ii}} & \mathbf{0} \\ \mathbf{0} & \bar{\mathbf{K}}_{\mathbf{bb}} \end{bmatrix} \begin{Bmatrix} \mathbf{q}_{\mathrm{i}} \\ \mathbf{u}_{\mathrm{pre}} \end{Bmatrix} + \begin{Bmatrix} \mathbf{0} \\ \mathbf{F}_{\mathrm{J,b}}(\mathbf{u}_{\mathrm{pre}}) \end{Bmatrix} = \begin{Bmatrix} \mathbf{0} \\ \mathbf{F}_{\mathrm{pre}} \end{Bmatrix} \tag{6}$$

The joint force, $\mathbf{F}_J(\mathbf{u})$, is modeled here using the node-to-node penalty stiffness method using either normal gap elements or triaxial gap elements. The former only applies penalty stiffness in the direction normal to the contact surface, whereas the triaxial spring applies additional in-plane stiffness when a contact gap closes. Consider the node pair, j, such that the normal gap is computed as,

$$g^j = \left(Z_1^j - \Delta Z_1^j\right) - \left(Z_2^j - \Delta Z_2^j\right) \tag{7}$$

where Z is the undeformed normal coordinate and ΔZ is the relative normal displacement. The penalty spring method defines the normal contact force for the j[th] node pair as,

$$F_Z^j = \begin{cases} k_z g^j & g^j < 0 \\ 0, & g^j \geq 0 \end{cases} \tag{8}$$

The normal penalty spring stiffness is denoted as k_z. For the triaxial penalty spring, an in-plane stiffness term is included, with in-plane penalty stiffnesses k_x and k_y,

$$F_X^j = \begin{cases} k_x \Delta X & g^j < 0 \\ 0, & g^j \geq 0 \end{cases} \tag{9}$$

$$F_Y^j = \begin{cases} k_y \Delta Y & g^j < 0 \\ 0, & g^j \geq 0 \end{cases} \tag{10}$$

Following the quasi-static preload analysis of the model in Eq. 5 the model is linearized about this equilibrium state yielding,

$$\begin{bmatrix} \mathbf{I} & \bar{\mathbf{M}}_{\mathbf{ib}} \\ \bar{\mathbf{M}}_{\mathbf{bi}} & \bar{\mathbf{M}}_{\mathbf{bb}} \end{bmatrix} \begin{Bmatrix} \ddot{\mathbf{q}}_{\mathrm{i}} \\ \ddot{\mathbf{u}}_{\mathrm{b}} \end{Bmatrix} + \begin{bmatrix} \boldsymbol{\Lambda}_{\mathbf{ii}} & \mathbf{0} \\ \mathbf{0} & \bar{\mathbf{K}}_{\mathbf{bb}} + \frac{\partial \mathbf{F_j}}{\partial \mathbf{u_b}}\Big|_{\mathbf{u_{pre}}} \end{bmatrix} \begin{Bmatrix} \mathbf{q}_{\mathrm{i}} \\ \mathbf{u}_{\mathrm{b}} \end{Bmatrix} = \begin{Bmatrix} \mathbf{0} \\ \bar{\mathbf{F}}_{\mathbf{b}} \end{Bmatrix} \tag{11}$$

Note that the bar above the mass and stiffness terms indicates the transformed HCB model and the partial derivative of the nonlinear force added to the HCB stiffness matrix at the boundary DOF represents the stiffness of the joint in either a fully stuck state in the case of the triaxial penalty spring, or a fully slipped state for the normal penalty springs.

2.2 System Level Characteristic Constraint Reduction (S-CC)

The application of the System Level Characteristic Constraint (S-CC) interface reduction further reduces the linearized Hurty/Craig Bampton ROM in Eq. 11. This approach computes the eigenvectors from the boundary partition of the linearized HCB model and uses a truncated set of the S-CC modes as a basis for the reduction [9], [14]. The modes are computed about the linearized state, and the subscript CC denotes characteristic constraint modes,

$$\left(\mathbf{K}_{\mathbf{bb}} + \frac{\partial \mathbf{F_j}}{\partial \mathbf{u_b}}\Big|_{\mathbf{u_{pre}}} - \omega_{\mathrm{CC}}^2 \mathbf{M}_{\mathbf{bb}}\right) \boldsymbol{\Phi}_{\mathbf{CC}} = \mathbf{0} \tag{12}$$

Depending on the type of penalty springs used to linearize the system, this equation produces either the fully stuck or fully slipping S-CC modes. A truncated subset of the S-CC modes is used to further reduce the HCB mass and stiffness matrices using the transformation matrix,

$$[\mathbf{T}_{\mathbf{SCC}}] = \begin{bmatrix} \mathbf{I} & \mathbf{0} \\ \mathbf{0} & \boldsymbol{\Phi}_{\mathbf{CC}} \end{bmatrix} \tag{13}$$

$$\mathbf{M_{SCC}} = [\mathbf{T_{SCC}}]^{\mathbf{T}} \begin{bmatrix} \mathbf{I} & \bar{\mathbf{M}}_{\mathbf{ib}} \\ \bar{\mathbf{M}}_{\mathbf{bi}} & \bar{\mathbf{M}}_{\mathbf{bb}} \end{bmatrix} [\mathbf{T_{SCC}}] \tag{14}$$

$$\mathbf{K_{SCC}} = [\mathbf{T_{SCC}}]^{\mathbf{T}} \begin{bmatrix} \mathbf{\Lambda_{ii}} & \mathbf{0} \\ \mathbf{0} & \bar{\mathbf{K}}_{\mathbf{bb}} + \frac{\partial \mathbf{F_j}}{\partial \mathbf{u_b}}\Big|_{\mathbf{u_{pre}}} \end{bmatrix} [\mathbf{T_{SCC}}] \tag{15}$$

If all CC modes are kept in the reduction, the S-CC model is identical to the HCB reduced model. This reduction method captures both the motion of the boundary and the global dynamics of the structure, resulting in a significant reduction in the number of DOF in the FEM. Utilizing the linearized EOM from the preloaded state in Eq. 11, the EOM for the S-CC reduced model about the nonlinear preloaded state is,

$$\begin{bmatrix} \mathbf{I} & \bar{\mathbf{M}}_{\mathbf{ic}} \\ \bar{\mathbf{M}}_{\mathbf{ci}} & \bar{\mathbf{M}}_{\mathbf{cc}} \end{bmatrix} \begin{Bmatrix} \ddot{\mathbf{q}}_{\mathbf{i}} \\ \ddot{\mathbf{q}}_{\mathbf{cc}} \end{Bmatrix} + \begin{bmatrix} \mathbf{\Lambda_{ii}} & \mathbf{0} \\ \mathbf{0} & \mathbf{\Lambda_{cc}} \end{bmatrix} \begin{Bmatrix} \mathbf{q}_{\mathbf{i}} \\ \mathbf{q}_{\mathbf{cc}} \end{Bmatrix} = \bar{\mathbf{f}}(\mathbf{t}) \tag{16}$$

where the c subscript indicates the reduction using CC modes. The stiffness matrix is completely decoupled with Λ_{cc} thanks to the orthogonality properties of the eigenvectors. At this point, a nonlinear modal Iwan element is placed between the S-CC shape and the ground to evaluate the effectiveness of the nonlinear ROM (NLROM) to generate amplitude dependent modal parameter curves. The following subsections describe the theory and the usage of the NLROM.

2.3 Whole-joint Model

Segalman's 4-parameter Iwan element was developed as part of a large research effort at Sandia National Laboratories that considered both analytical solutions for contact and empirical evidence that showed that joints exhibit power-law energy dissipation versus force (or vibration amplitude) [3]. An Iwan element is a collection of slider or Jenkins elements in parallel, in which the slip force[3] for each slider is chosen to create an element that exhibits power-law energy dissipation. This approach simplifies joint modeling significantly; a full finite element model of a joint must consider every point in the interface to be independent and goverened by several parameters, i.e. the friction coefficient, normal force, etc…. When one multiplies these unknowns by the number of contact nodes there may be hundreds or thousands of free parameters. Segalman's model recognizes that the net effect of all of these parameters must be to produce power-law dissipation versus vibration amplitude, which is goverened by only two of the four parameters in the Iwan model. The other two parameters control the transition to macro-slip when the joint slips completely. Macro-slip is typically not observed in engineered joints if they are tightened properly, except perhaps under extreme loading.

The four parameter Iwan model can be represented by the parameters: $F_s, K_T, \chi, \text{and } \beta$, given in Table 1. For an in-depth discussion of the Iwan element, refer to Segalman's original paper on Iwan elements [3] and Deaner's paper on the modal Iwan model [14].

Table 1: Definition of Iwan Parameters (physical description)

F_s	The force necessary to cause macroslip
K_T	The tangential stiffness of the Jenkins elements (i.e. the joint stiffness when no slip occurs)
χ	The exponent that describes the slope of the energy dissipation curve

[3] If all sliders have the same friction coefficient then the slip force is defined by the normal force for each slider.

β	The ratio of the number of Jenkins elements that slip before micro-slip and then at macroslip

This element is connected between every necessary S-CC mode of the NLROM and the ground to enable the model to generate curves that depict the amplitude dependent trends of the natural frequency and damping of the global mode. However, a model with an Iwan joint cannot generate these curves for different load steps without a dynamic or quasi-static analysis. For this paper, the quasi-static method is utilized. It is important to note that adding these elements to S-CC shapes allows the modes of the system to retain some level of coupling.

2.4 Adding the S-CC Iwan Element

As given by Eq. 16, when the HCB model is transformed to S-CC space assuming the interface is fully stuck, the stiffness matrix is diagonalized with the S-CC shape stiffnesses due to the orthogonality properties of the modes. A four-parameter modal Iwan element is appended to the linearize equations in Eq. 16 in order to capture the effect of the joint when the structure is loaded in the shape of the S-CC mode. In the case where the joint is modeled as a normal penalty spring (i.e. fully slipped), the bolts are the only source of in-plane stiffness, and the linearized natural frequency for the ith S-CC mode shape is denoted as $\omega^2_{\mathrm{CC},i,\infty}$. Conversely, when the interface is fully stuck, the linearized frequency is $\omega^2_{\mathrm{CC},i}$. Appending a modal Iwan element to an S-CC coordinate in Eq. 16 (and neglecting the inertia terms) results in,

$$\omega^2_{\mathrm{CC},i,\infty}\mathrm{q}_{\mathrm{cc,i}} + \bar{f}_{\mathrm{CC,i}}\left(\mathrm{q}_{\mathrm{cc,i}}\right) = \bar{\mathrm{f}}_i(\mathrm{t}) \tag{17}$$

where $\bar{f}_{\mathrm{CC,i}}\left(\mathrm{q}_{\mathrm{cc,i}}\right)$ is the modal Iwan element applied to the ith S-CC coordinate. The modal Iwan joint has a linearized stiffness associated with it, termed $\mathrm{K_T}$, which can be chosen such that $\boldsymbol{\Lambda_{cc}}|_{\boldsymbol{i}} = \omega^2_{\mathrm{CC},i,\infty} + \mathrm{K_T}$. This constraint is placed on the selection such that the modes 1.) converge to the fully stuck solution at low response amplitudes, and 2.) converge to the fully slipped solution at high response amplitude as the stiffness of the modal Iwan element goes to zero. In this approach, the interface DOF may be reduced while maintaining flexibility in the boundary DOF and spanning all the possible joints in the structure. The resulting nonlinear equations-of-motion with grounded S-CC modal Iwan elements becomes,

$$\begin{bmatrix} \mathbf{I} & \bar{\mathbf{M}}_{\mathbf{ic}} \\ \bar{\mathbf{M}}_{\mathbf{ci}} & \bar{\mathbf{M}}_{\mathbf{cc}} \end{bmatrix} \begin{Bmatrix} \ddot{\mathbf{q}}_{\mathrm{i}} \\ \ddot{\mathbf{q}}_{\mathrm{cc}} \end{Bmatrix} + \begin{bmatrix} \boldsymbol{\Lambda}_{\mathbf{ii}} & \mathbf{0} \\ \mathbf{0} & \boldsymbol{\Lambda}_{\mathbf{cc},\infty} \end{bmatrix} \begin{Bmatrix} \mathbf{q}_{\mathbf{i}} \\ \mathbf{q}_{\mathbf{cc}} \end{Bmatrix} + \begin{Bmatrix} \mathbf{0} \\ \bar{\mathbf{f}}_{\mathrm{CC}}(\mathbf{q}_{\mathrm{cc}}) \end{Bmatrix} = \begin{Bmatrix} \mathbf{0} \\ \bar{\mathbf{f}}(\mathbf{t}) \end{Bmatrix} \tag{18}$$

2.5 Quasi-Static Modal Analysis (QSMA)

Quasi-Static Modal Analysis (QSMA) was originally proposed by Festjens et. al [4] as a method that replaces a dynamic simulation of a joint with a quasi-static problem that can be solved to estimate the effective natural frequency and damping of a single mode due to the joints in the structure. A quasi-static distributed force is applied that replicates the inertial loading experienced during vibration in that mode and coupling between the vibration modes is ignored. Lacayo and Allen further extended QSMA, developing an even faster algorithm for the case where the joints are represented by Iwan elements [5]. The theory is presented in depth in that paper and for brevity it will not be repeated here other than key points. This paper extends the usage of QSMA to the S-CC NLROM. The S-CC model still has the general form given in Eq. 16, and the nonlinear joints can be represented through a nonlinear force $\mathbf{F}_J(\mathbf{u})$ as shown in Eq. 19.

$$\mathbf{M_{SCC}}\ddot{\mathbf{u}} + \mathbf{K_{SCC}}\mathbf{u} + \mathbf{F}_J(\mathbf{u}) = \mathbf{F} \tag{19}$$

QSMA consists of solving the equation above for a static case, i.e. $\ddot{\boldsymbol{u}} = 0$, where the forcing is $\mathbf{F} = \alpha[\mathbf{M}]\boldsymbol{\varphi}_i$. In this case, the nonlinear joint force is the result of the Iwan element at different displacements, u, based

on α. After solving Eq. 19, one obtains the static response, $\mathbf{u}(\alpha)$, from which the modal velocity amplitude, natural frequency, and damping ratio can be written as function of α as shown in Eq. 12-17 in [5]. The damping ratio is obtained by adding up the energy dissipated by friction from each Iwan joint in the system. Given that all three variables are functions of amplitude, the damping and natural frequency can be plotted in terms of modal velocity amplitude and this is the convention that will be used in this work.

3. APPLICATION TO S4 BEAM: EVALUATION OF LINEAR REDUCTION METHODS

The finite element model of the S4 Beam is reduced to a Hurty/Craig-Bampton model with 20 fixed interface modes and all of the nodes at the interfaces between the beams (3680 DOF), plus four additional points at which the preload is applied. The boundary DOF of the HCB model are shown in Figure 2. The boundary DOF are kept to maintain node-to-node contact in the HCB model using both the normal and triaxial penalty stiffness methods. The contact areas are shown separated for ease of visualization but are coincident in the model. It is important to note that the beams have pinned boundary conditions at the ends of the bottom beams.

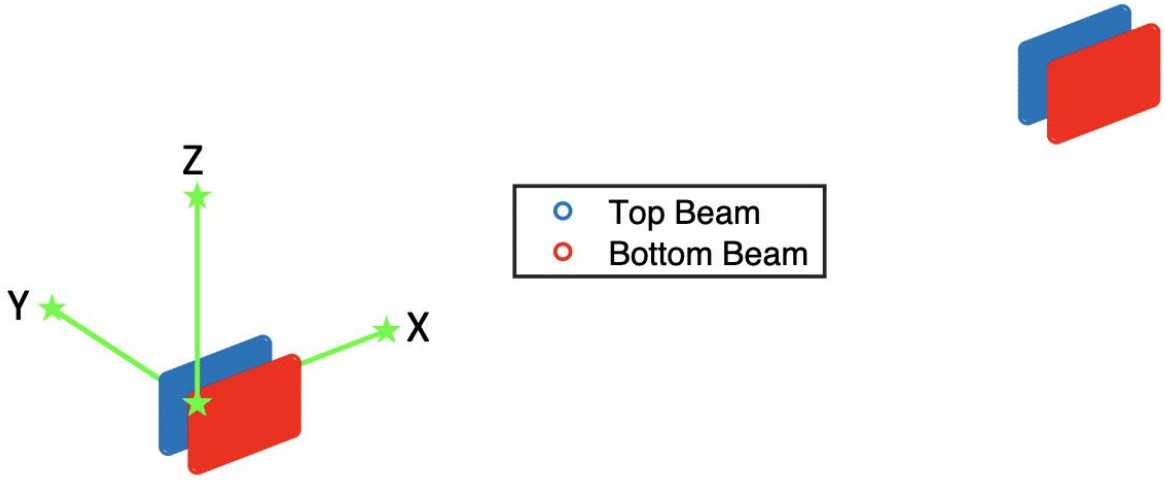

Figure 2: HCB reduced finite element model of the S4B depicting the coordinate system

A preload analysis using the penalty spring method was done on the HCB model to determine the DOF in contact between the interfaces. Figure 3 shows the normal contact force at the interface for the preload for each of the nodes on the bottom beam for the left and right interface. All nodes with a nonzero preload force are considered to be nodes in contact. The 2D representation is color coded with the brightest areas corresponding to the largest preload force, and the 3D representation is meshed through Delaunay Triangulation. The nonlinear preload analysis performed in [8] did not include the effect of friction and only applied the preload using a penalty spring normal to the contact surface. However, modeling friction is necessary, or the final model will not contain the desired physics. As a result, triaxial penalty springs were added to the model to provide the additional constraint that would be imposed by contact in the in-plane directions. Similar to a uniaxial spring, triaxial springs are added at each set of x, and z DOF respectively in the Jacobian from Eq. 11 to obtain a preloaded model. This method is an extension of Hughes et. al, where now additional constraints are only added to the nodes in contact [8]. As a result, arbitrarily selected penalty spring constants of 1e5 N/m, 1e10 N/m, and 1e5 N/m for the x, y, and z directions respectively were applied to the FEM between all of the interface nodes that were in contact.

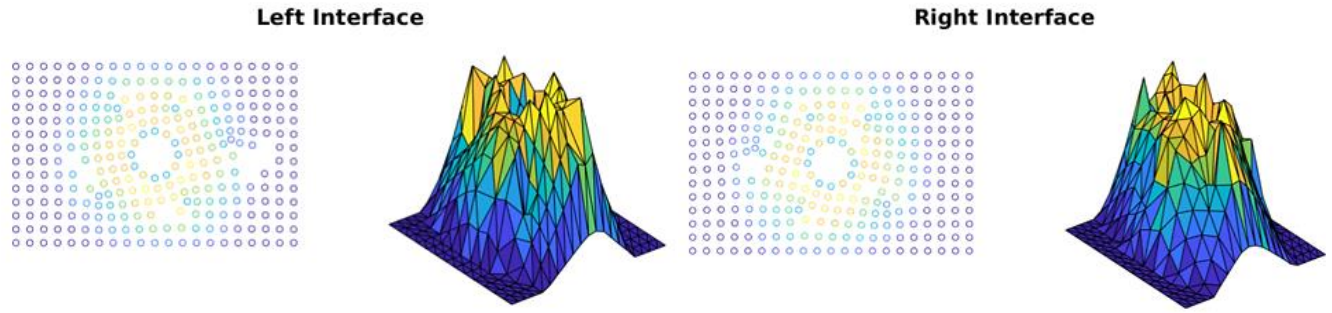

Figure 3: (Left) Left bottom interface of the beam, (Right) Right bottom interface of the beam. First figure is the nodes in a 2D scatter representation, and the second figure is the nodes in contact in a 3D representation

A preloaded FEM with preload and in-plane penalty springs denotes the fully stuck case where the two components of the FEM are held tightly together and experience no slip for nodes that have a closed contact gap. The fully slipped case has no in-plane contribution from the preload force term in Eq. 11, and the bolts are the only contribution to the in-plane stiffness. Table 2 denotes the frequencies for the first six elastic modes in the fully slipped case versus the fully stuck case. It is evident that with the addition of the preload, the frequencies increase due to the stiffened interface. For all subsequent results in this section, the preload contribution to the ROM is considered.

Table 2: Fully slipped interface vs. fully stuck interface frequencies incorporating the nonlinear preload force term

Mode	Fully Slipped Model Frequency (Hz)	Fully Stuck Model Frequency (Hz)
1	113.99	132.83
2	150.2	249.15
3	242.54	275.02
4	306.7	317.83
5	335.51	384.89
6	460.68	578.36

A secondary HCB reduction was done on the interface to reduce from the full interface DOF to the DOF of the interface that are in contact as established from the preload analysis. Using 20 fixed interface modes, this reduces the DOF of the model from 3684 to 3594 contact DOF with no considerable frequency error, while preserving the linear mode shapes. The secondary HCB reduced model will be used for all subsequent results.

Although 3594 DOF is a relatively small model, this number of DOF would still be quite cumbersome if one was to apply a linear spring or physical nonlinear Iwan element which require a joint element at every DOF. To circumvent this issue, the S-CC reduction and Coppolino reduction (refer to the Appendix) techniques were evaluated on this structure. The primary metric of comparing the results is the frequency error against the full HCB model (with no interface reduction) and the modal assurance criterion (MAC) to compare mode shapes [15]. Using the methods discussed in Section 2.2, Table 3 below depicts the frequency error for various number of S-CC shapes utilized for the fully stuck case.

Table 3: Frequency errors from the S-CC reduction using a range of S-CC shapes against the fully stuck model HCB frequencies for the first six modes

Mode	ROM Modal Frequency (Hz)	1 S-CC Shapes Freq. Error	4 S-CC Shapes Freq. Error	6 S-CC Shapes Freq. Error	
1	132.83	0.0015%	0.0009%	0.0005%	**Using 14 S-CC shapes gives 10 modes with Freq. Error below 1%**
2	249.15	15.55%	0.003%	0.0006%	
3	275.02	186.9%	4.68%	0.097%	
4	317.83	148.62%	0.019%	0.002%	
5	384.89	106.85%	0.018%	0.001%	
6	578.39	50.57%	36.61%	0.07%	

This result shows that six S-CC shapes are required to capture the first six modes with less than 0.1% frequency error. This effectively reduces the number of DOF from 3594 to 26, including 20 fixed interface modes and 6 S-CC DOF. Figure 4 shows a comparison of the modes of the system reduced using the S-CC method against the HCB model using the Modal Assurance Criterion (MAC). It is important to note that since the model was reduced to the interface DOF only, the DOF set is not sufficient to distinguish all of the modes and large off diagonal terms are present for some combinations of modes.

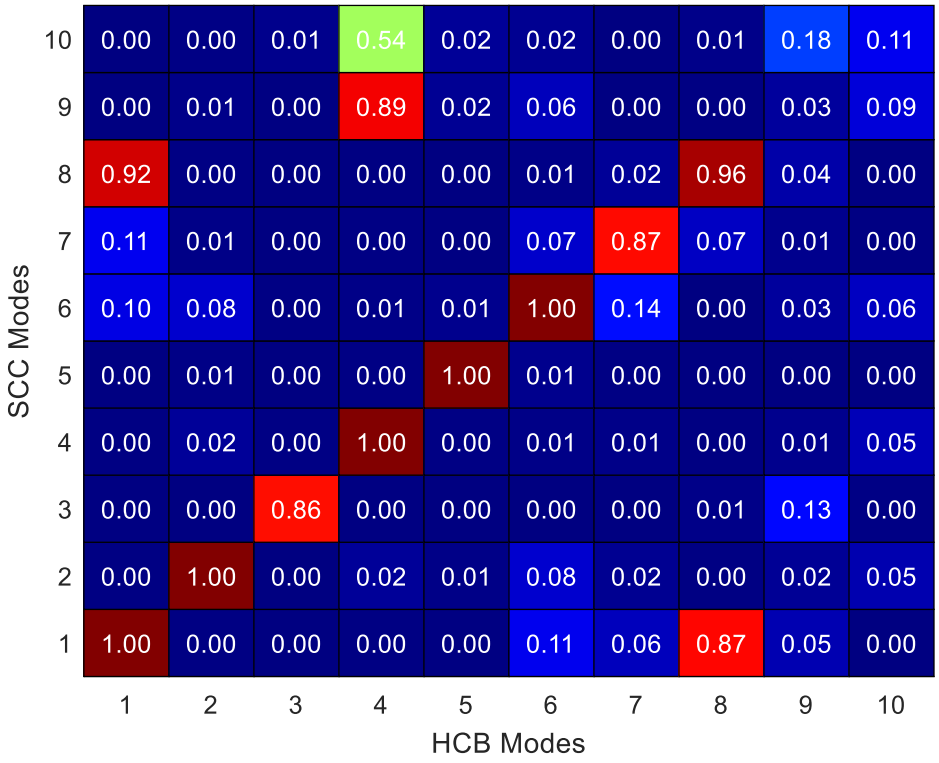

Figure 4: Visual representation of the MAC between the S-CC reduced modes and the HCB reduced modes

The MAC shows good correlation for the first 7 modes, indicating that the mode shapes of the structure are preserved through this reduction. A convergence study was used to verify the decrease in frequency error with an increase in the number of S-CC shapes preserved, as shown in Figure 5. At 17 S-CC shapes, the frequency errors are nearly converged with the largest errors in the sixth mode.

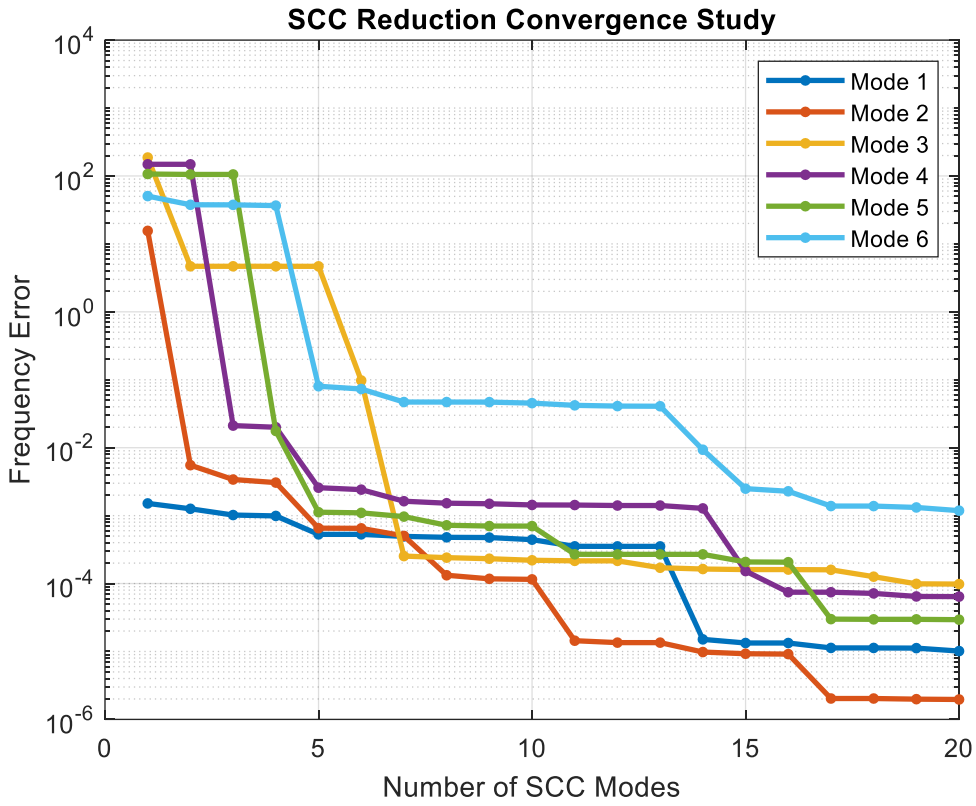

Figure 5: Convergence study of frequency error as a function of the number of S-CC shapes retained in the reduction

4. APPLICATION TO S4 BEAM: S-CC NONLINEAR ROM EVALUATION

Analogous to physical Iwan elements, in the proposed approach the Iwan elements are placed between an S-CC modal coordinate, $\mathbf{q_{cc}}$, and the ground to capture slip in the joint as the participation of that interface shape increases in the response. The parameters used in this case study are approximated from [6] for the Full – Rbar model of a free-free S4 Beam, and are given in Table 4. K_T is variable for each S-CC shape, chosen to replicate the difference in stiffness of each S-CC shape as the system goes from fully stuck to fully slipping, as detailed in Section 2.4. Although the system studied here has different boundary conditions (pinned-pinned), these parameters should produce a physically plausible system. The focus will be on verifying that reasonable frequency and damping versus amplitude curves can be obtained with this method and to examine the coupling of the S-CC shapes. A future work will extend this to calibrate the parameters of the joints to replicate measurements from a real system.

Table 4: Physical Iwan parameters used for the truth model

F_s	0.5
K_T	*Variable*
χ	-0.2
β	2.5

At first an Iwan element with identical parameters is placed between each S-CC coordinate and the ground. This model is then solved using QSMA to generate the amplitude dependent frequency and damping for the first six vibration modes of the S4 beam; these curves are shown in Figure 6. The left figure shows the percent frequency shift as a function of modal displacement amplitude and the right figure shows the damping ratio of each mode as a function of modal displacement amplitude. Since the linearized frequencies and mode shapes are preserved during the S-CC linear reduction, as shown in Section 3, the model performs well by converging to the linearized state at low modal displacement amplitudes. The nonlinear frequency and damping curves each exhibit different shifts for the case of S-CC Iwan parameters used. It is expected that different combinations of parameters would change these curves, which would be important for future calibration studies.

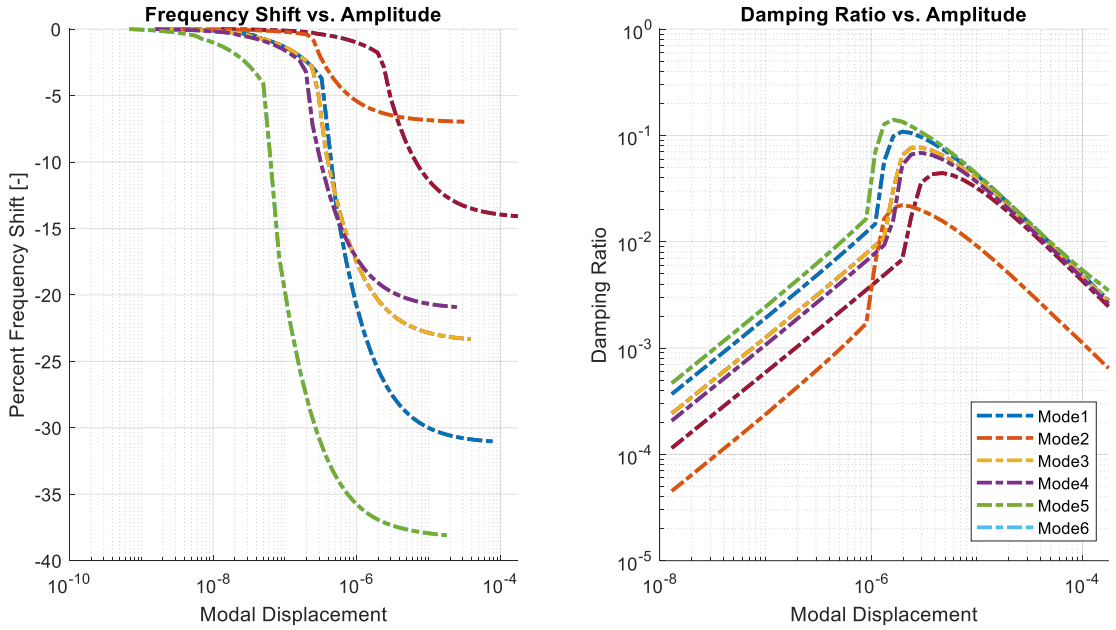

Figure 6: Frequency and damping vs. amplitude curves for all 6 modes of interest utilizing 6 S-CC shapes

In practice, it may not be desirable to place an Iwan element at every S-CC coordinate since not all shapes are expected to influence the nonlinear modal response. Hence, a sensitivity analysis is necessary to understand which S-CC shape influences the nonlinear mode of the system. Prior to the sensitivity analysis, it is important to distinguish the difference between an S-CC shape and the global mode shape of the structure. Figure 7 shows the first three mode shapes of the assembled system (however, only the interface DOF are retained and so these are visualized using only those DOF). Figure 8 shows the first three S-CC shapes, which are only defined at the interface DOF and hence are complete.

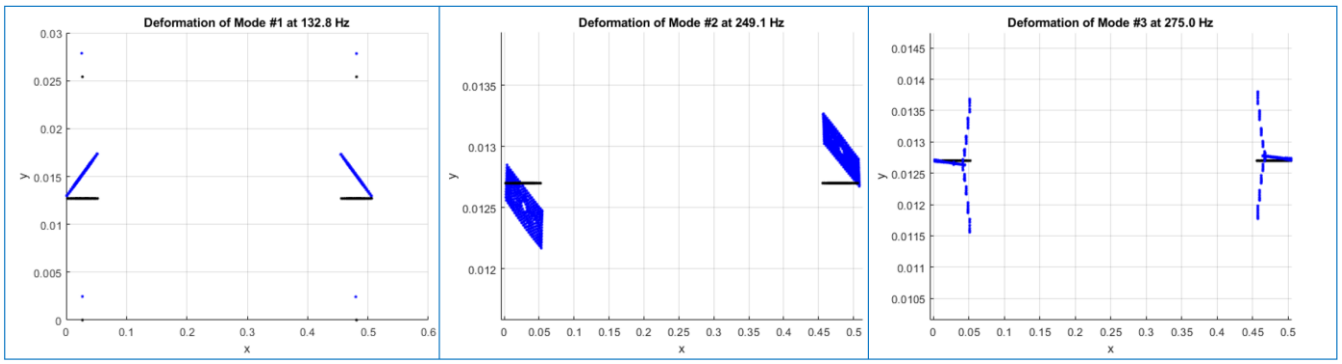

Figure 7: First 3 HCB reduced mode shapes of the interface

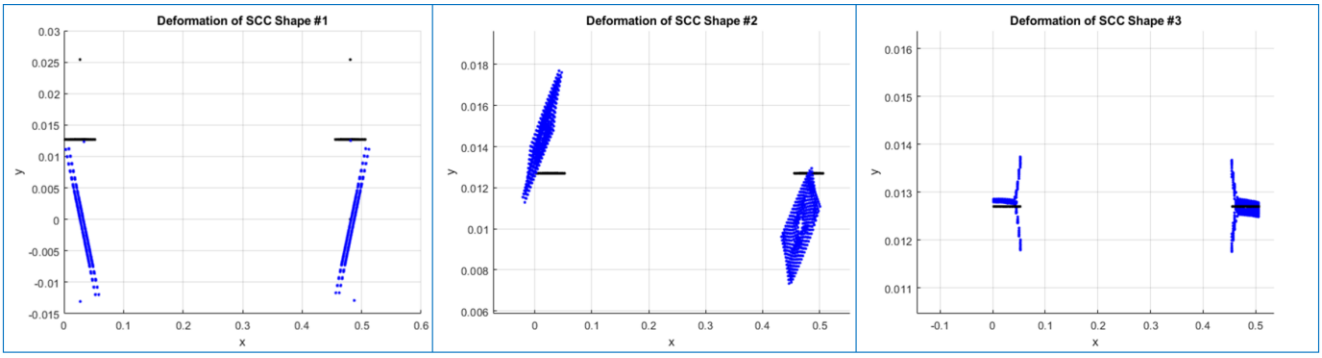

Figure 8: First 3 S-CC deformation shapes

Interestingly, the S-CC shapes look nearly identical to the global mode shapes. This is perhaps to be expected since the S-CC shapes are found by statically reducing the whole system to the interface DOF and then solving for the modes. However, one must recall that the S-CC modes are not the same as the system modes, and each system mode may involve participation from multiple mode shapes. This is shown in Figure 9 where each column is the global mode shape and each row denotes the S-CC contribution to that mode shape. It is important to note that each column is normalized to a max value of one. Here 14 S-CC shapes are examined to see if there is higher degree coupling between the S-CC shapes for each mode

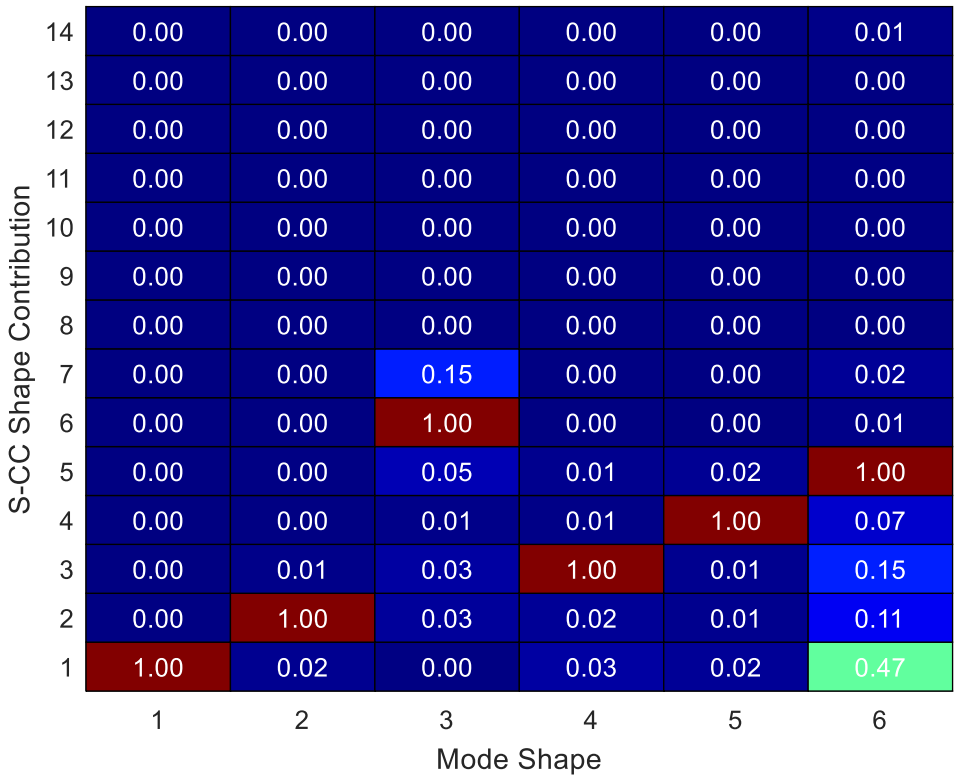

Figure 9: A portion of the S-CC mode shape matrix where each row is an S-CC shape and each column corresponds to the global mode shape.

Mode shapes 1 through 5 only rely on a single S-CC shape, whereas the 6th mode shape relies on a contribution of more than 10% from S-CC shapes 1,2 and 3 in addition to S-CC shape 5. These two differences can be examined in modes 1 and 6 in the figures below. Figure 10 depicts the change in frequency and damping with modal displacement amplitude for Mode 1 (132.83 Hz) for a range of Iwan elements. Each curve denotes a case study where an Iwan element was placed on the respective S-CC shape(s), with the remaining S-CC coordinates attached to the ground with a linear spring of value K_T. As a result, at low amplitudes the modes should converge to the linear frequency of the fully stuck case.

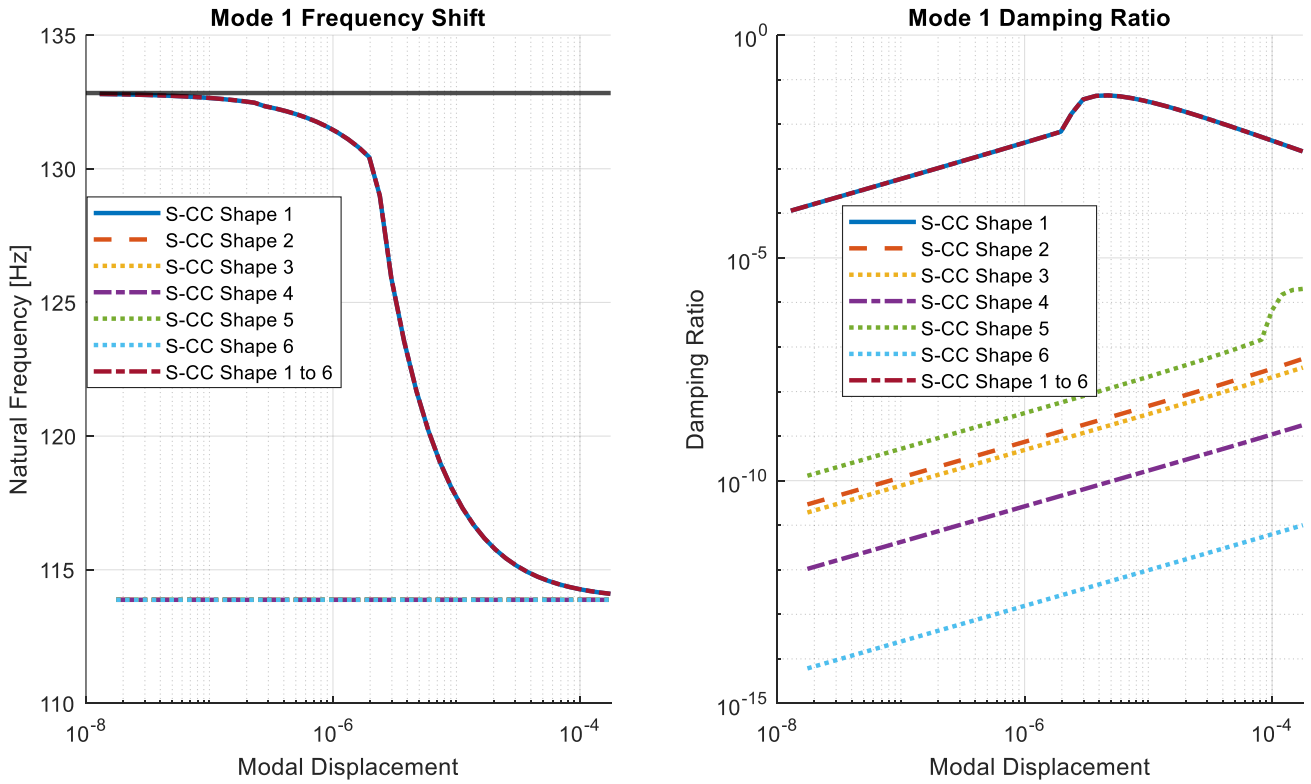

Figure 10: Frequency and damping vs. amplitude curves for Mode 1

As expected from the sensitivity analysis, the results show that if Mode 1 is the primary mode of interest, it is not necessary to place an Iwan element at each S-CC shape, only those that pertain to the motion of the mode since the linear element accounts for the additional stiffness added to each mode. Although each S-CC shape can be used to produce frequency and damping curves, it is apparent that certain S-CC shapes cannot be used capture nonlinear effects. For Mode 1, Shapes 2 – 6 have no contribution toward capturing nonlinearity of the mode, and therefore do not require an Iwan element.

On the other hand, Mode 6 (578.39 Hz) has a contribution from more than one S-CC shape as shown in Figure 11. With an Iwan placed on a single S-CC coordinate, only S-CC shape 5 can capture the majority of the dynamics of the mode. However, at higher amplitudes the shape begins to underpredict the response based on the curve utilizing all six S-CC shapes. Therefore, to accurately capture the behavior of Mode 6, an Iwan element is necessary at S-CC shapes 1, 2, 3, and 5. The results for the other four modes of interest is replicated in the Appendix.

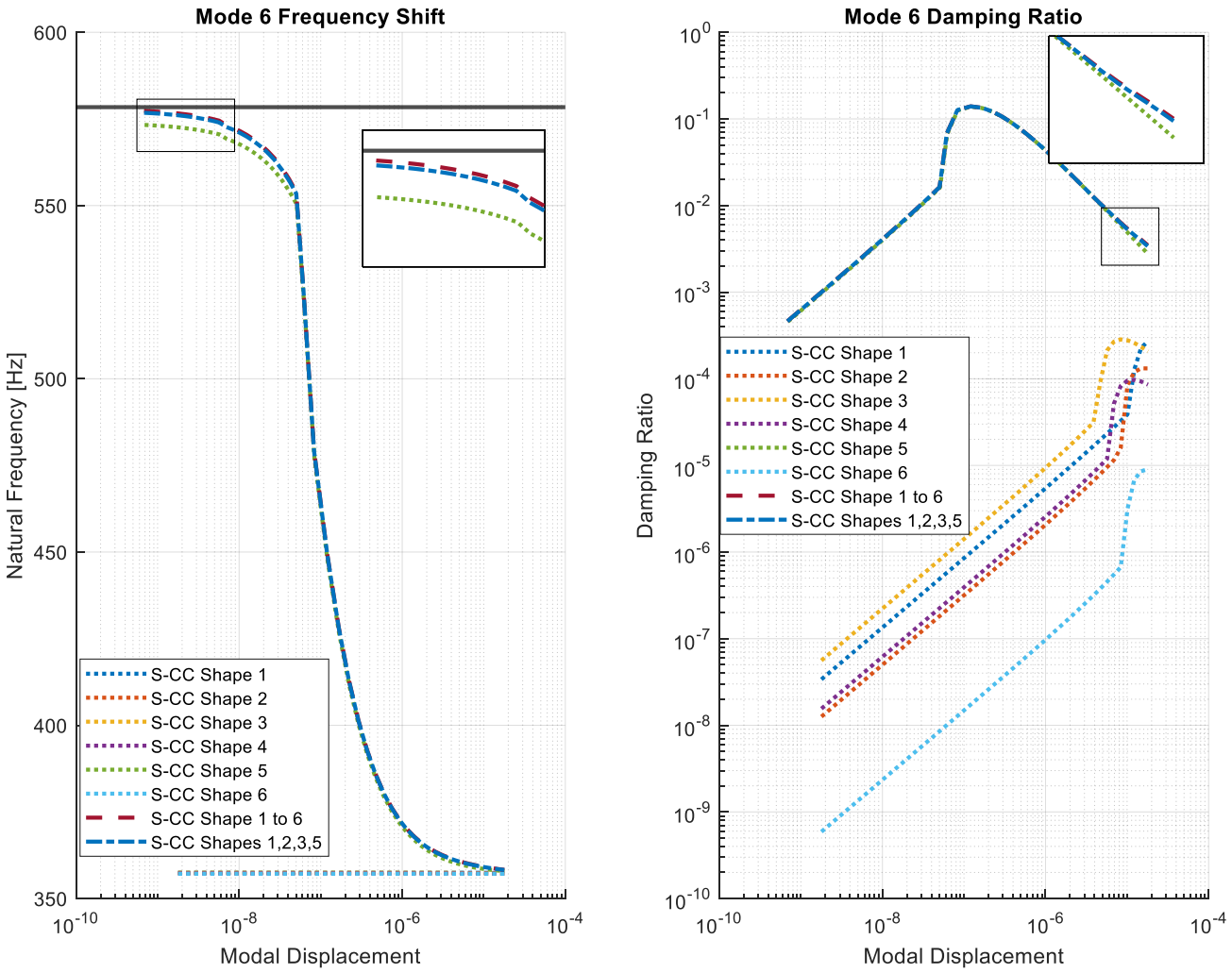

Figure 11: Frequency and damping vs. amplitude curves for Mode 6

5. CONCLUSION

This paper explored a new way of representing the linear and nonlinear properties of joints in the nonlinear benchmark structure, the S4 Beam, utilizing the S-CC reduction technique. Traditionally high-fidelity models were created using RBAR and RBE3 spidered joints to understand the joint behavior. This paper studied reduction techniques that maintained the flexibility of the interface to an even greater degree than the RBE3 spidering approach, while reducing the number of interface DOF. The viability these approaches was studied by evaluating their ability to reproduce the linear natural frequencies of the assembled HCB model after preload and their ability to capture the amplitude dependent frequency and damping caused by the joints.

The linear reduction methods showed that the S-CC reduction could accurately capture the frequency of the HCB interface model within 0.1% while maintaining accuracy of the mode shapes with a reduction of DOF by a factor of 1000.

The S-CC reduction technique was then evaluated with Iwan elements to show that amplitude dependent frequency and damping curves could be constructed with an arbitrary set of Iwan parameters for the six modes of interest. It was shown that a nonlinear element is only necessary on the S-CC shape if the global bending mode activated that S-CC shape. When a bending mode only activates one S-CC shape, then that mode can only be affected that if an S-CC shape is added to that mode shape. It was shown through a sensitivity analysis that some modes, such as mode 6, require more than one S-CC shape to accurately capture the nonlinear dynamics.

In future work, additional reduction methods such as the Coppolino method will be extended with nonlinear elements for nonlinear calibration. It is also desired to evaluate these methods with an experimental truth model to see if these ROMs can be calibrated to curves obtained from the Hilbert Transform of experimental time histories. The hope is that the additional inherent flexibility of these reduced models will make it easier to update the FEM to reproduce the response of the measured system.

Acknowledgements

The views expressed in the article do not necessarily represent the views of the U.S. Department of Energy or the United States Government. Sandia National Laboratories is a multimission laboratory managed and operated by National Technology & Engineering Solutions of Sandia, LLC, a wholly owned subsidiary of Honeywell International Inc., for the U.S. Department of Energy's National Nuclear Security Administration under contract DE-NA0003525. SAND2019-12738 C

References

[1] "Abaqus analysis user's guide." Simulia, 2014.

[2] E. Jewell, M. S. Allen, and R. Lacayo, "Predicting damping of a cantilever beam with a bolted joint using quasi-static modal analysis," presented at the Proceedings of the ASME 2017 International Design Engineering Technical Conference & 13th International Conference on Multibody Systems, Nonlinear Dynamics, and Control IDETC/ MSNDC 2017, 2017.

[3] D. J. Segalman, "A Four-Parameter Iwan Model for Lap-Type Joints," *J. Appl. Mech.*, vol. 72, no. 5, pp. 752–760, Sep. 2005.

[4] H. Festjens, G. Chevallier, and J.-L. Dion, "A numerical quasi-static method for the identification of frictional dissipation in bolted joints," presented at the ASME 2012 International Design Engineering Technical Conferences and Computers and Information in Engineering Conference, IDETC/CIE 2012, August 12, 2012 - August 12, 2012, 2012, vol. 1, pp. 353–358.

[5] R. M. Lacayo and M. S. Allen, "Updating Structural Models Containing Nonlinear Iwan Joints Using Quasi-Static Modal Analysis," *Mech. Syst. Signal Process.*, vol. Volume 118, no. 1 March 2019, pp. 133–157, 2019.

[6] Aabhas Singh, Mitchell P. Wall, Matthew S. Allen, and Robert J. Kuether, "Spider Configurations for Models with Discrete Iwan Elements," in *Nonlinear Structures and Systems*, Orlando, Florida, 2019, vol. 1, pp. 25–38.

[7] A. Singh *et al.*, "Experimental Characterization of a new Benchmark Structure for Prediction of Damping Nonlinearity," presented at the 36th International Modal Analysis Conference (IMAC XXXVI), Orlando, Florida, 2018.

[8] Patrick J Hughes, Wensi Wu, and Wesley E Scott, "Interface Reduction on Hurty/Craig-Bampton Substructures with Frictionless Contact," in *Nonlinear Dynamics*, Orlando, FL, 2018, vol. 1, pp. 1–16.

[9] M. P. Castanier, Y. Tan, and C. Pierre, "Characteristic Constraint Modes for Component Mode Synthesis," *AIAA J.*, vol. 39, no. 6, pp. 1182–1187, 2001.

[10] R. N. Coppolino, “DOF Reduction Strategy for Large Order Finite Element Models,” in *Linking Models and Experiments*, 2011, vol. 2, pp. 359–366.
[11] R. J. Kuether, P. B. Coffin, and A. R. Brink, “ON HURTY/CRAIG-BAMPTON SUBSTRUCTURING WITH INTERFACE REDUCTION ON CONTACTING SURFACES,” in *International Design Engineering Technical Conferences*, Cleveland, Ohio, 2017.
[12] R. R. J. Craig and M. C. C. Bampton, “Coupling of Substructures for Dynamic Analysis,” *AIAA J.*, vol. 6, no. 7, pp. 1313–1319, 1968.
[13] D. Krattiger *et al.*, “Interface Reduction for Hurty/Craig-Bampton Substructured Models: Review and Improvement,” *Mech. Syst. Signal Process.*, vol. 114, pp. 579–605, Jan. 2019.
[14] B. Deaner, M. S. Allen, M. J. Starr, and D. J. Segalman, “Investigation of Modal Iwan Models for Structures with Bolted Joints,” presented at the 31st International Modal Analysis Conference (IMAC XXXI), 2013.
[15] R. J. Allemang and D. L. Brown, “A Correlation Coefficient for Modal Vector Analysis,” in *Proceedings*, 1982, pp. 110–116.

Appendix A: Additional Nonlinear Quasi-Static Curves

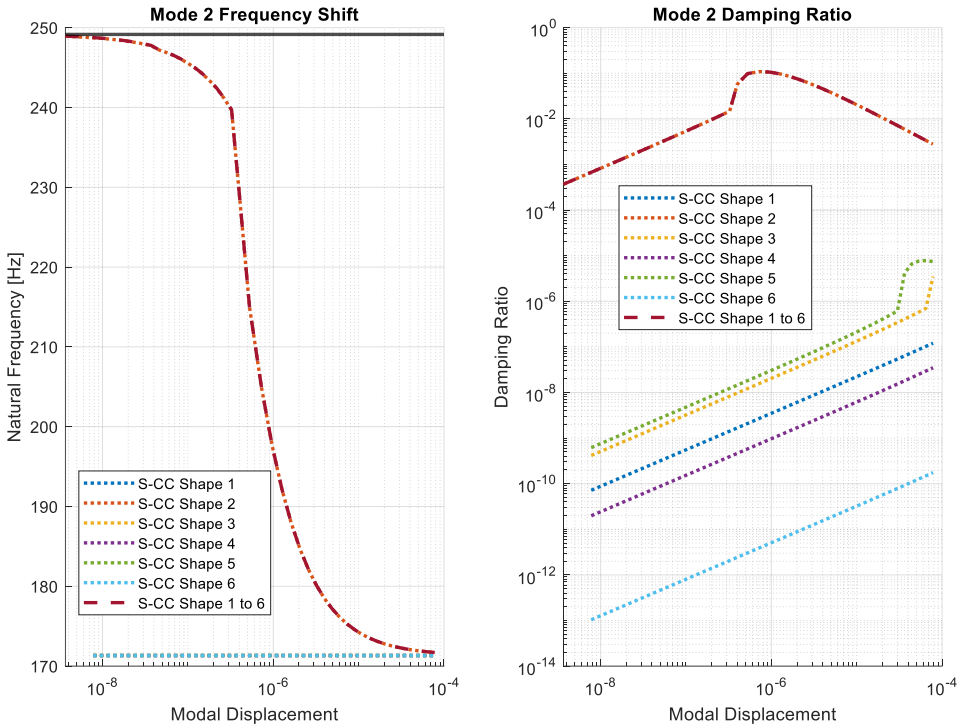

Figure A1: Frequency and damping vs. amplitude curves for Mode 2 with 1 through 6 S-CC shapes

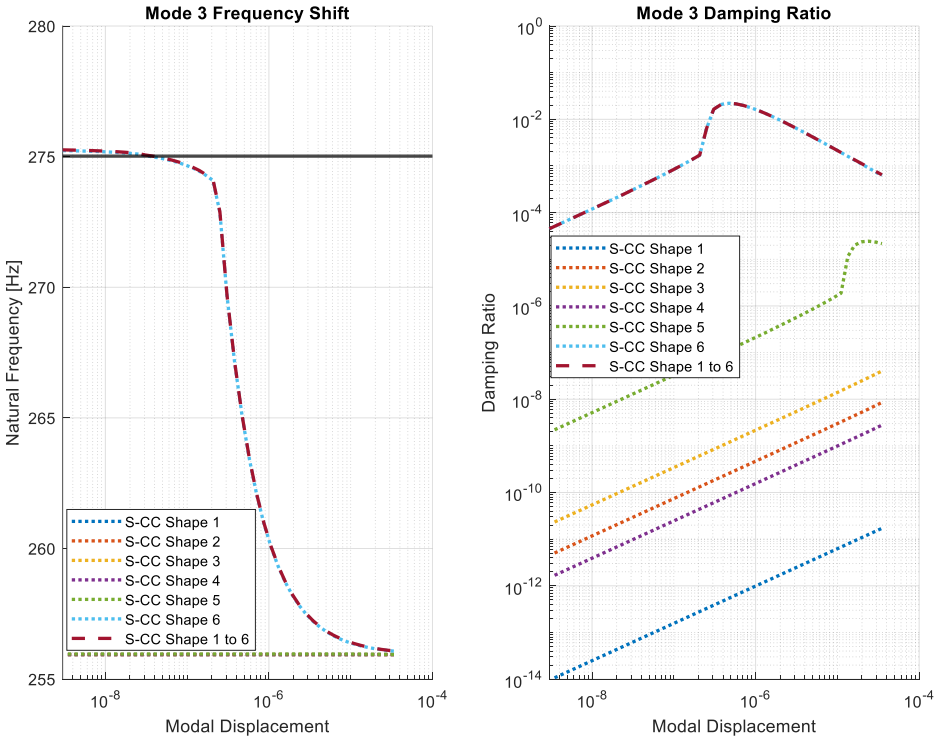

Figure A2: Frequency and damping vs. amplitude curves for Mode 3 with 1 through 6 S-CC shapes

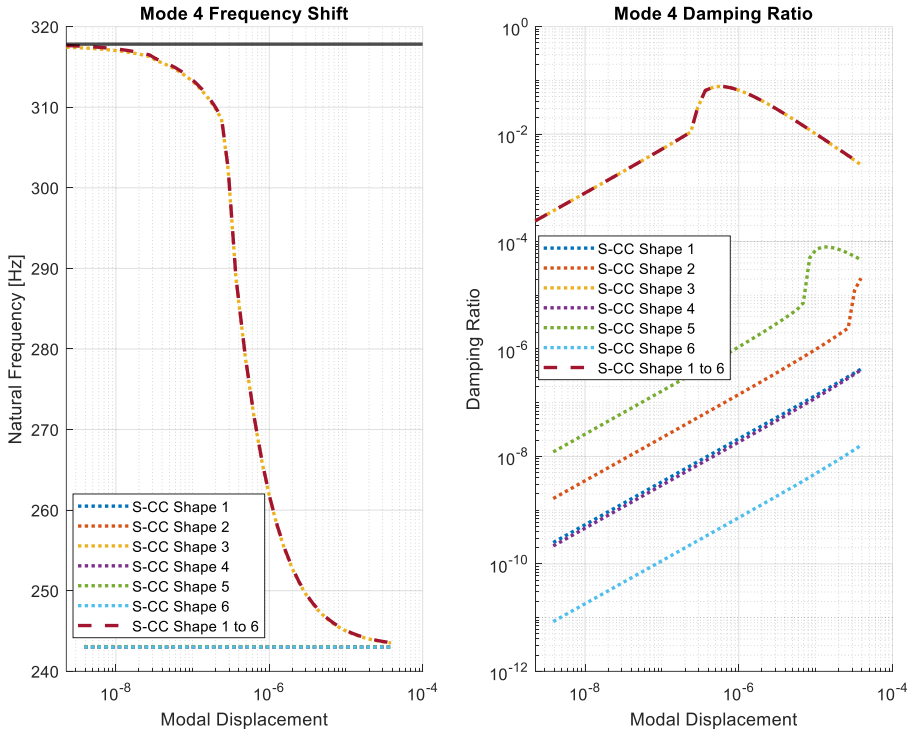

Figure A3: Frequency and damping vs. amplitude curves for Mode 4 with 1 through 6 S-CC shapes

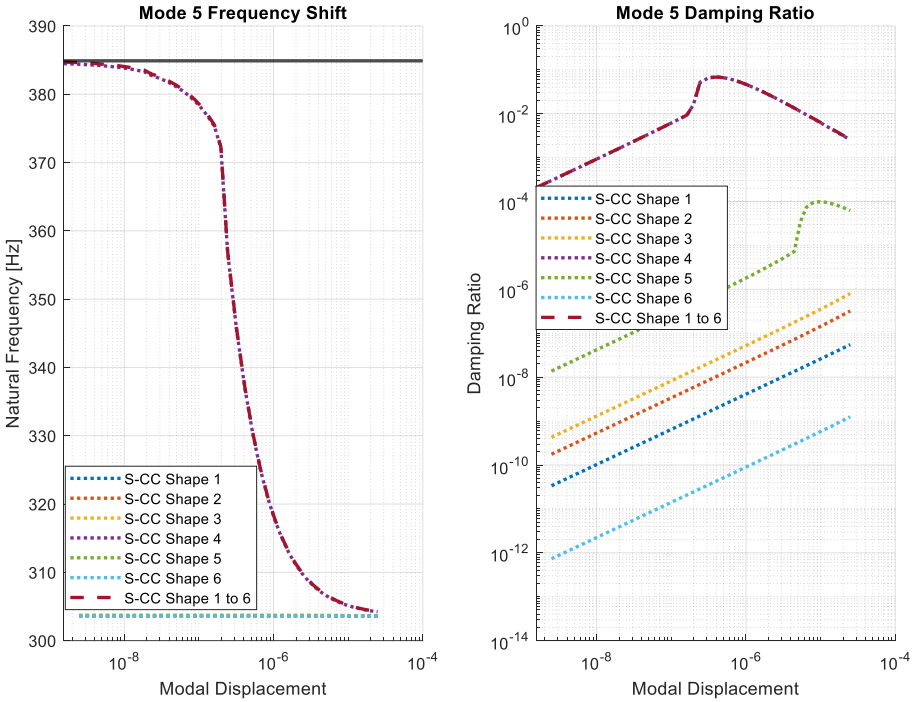

Figure A4: Frequency and damping vs. amplitude curves for Mode 5 with 1 through 6 S-CC shapes

Appendix B: Coppolino Reduction

6. Coppolino Reduction (COP) Theory

First introduced by Robert Coppolino, this reduction method was intended to extend Guyan Reduction past its inherent limitations on dynamic models with 3D elements [10]. Utilizing the static load basis as Ritz shape functions, Coppolino applies a unit rigid body displacement and rotation over a geometric patch of nodes as shown in Eq. 20 where $[\Psi]$ is the load patch matrix whose size is the number of DOF by number of rigid body modes used (typically six). If the contact interface is divided into n patches, then the number of columns increases to $6n$.

$$\{\mathbf{F}\} = [\Psi]\{\mathrm{F}_{\Psi}\} \tag{20}$$

This is then the foundation for the transformation matrix T from a mass and stiffness matrix to a Coppolino reduced mass and stiffness matrix as given in the equations below where Φ_{Copp} is the basis for reduction defined as $\Phi_{\mathrm{Copp}} = [\mathbf{K_{bb}}]^{-1}[\boldsymbol{\Psi}]$ with $\mathbf{K_{bb}}$ as the stiffness matrix partitioned to the boundary DOF.

$$\left[\mathbf{T_{copp}}\right] = \begin{bmatrix} \mathbf{I} & \mathbf{0} \\ \mathbf{0} & \boldsymbol{\Phi}_{\mathbf{Copp}} \end{bmatrix} \tag{21}$$

$$\mathbf{M_{copp}} = \left[\mathbf{T_{copp}}\right]^{\mathbf{T}}[\mathbf{M}]\left[\mathbf{T_{copp}}\right] \tag{22}$$

$$\mathbf{K_{copp}} = \left[\mathbf{T_{copp}}\right]^{\mathbf{T}}[\mathbf{K}]\left[\mathbf{T_{copp}}\right] \tag{23}$$

This linear model is evaluated in comparison to the S-CC approach to understand the linear behavior of the nonlinear ROM. This could then be extended to where nonlinear elements can be applied between the boundary DOF of the ROM can then be used to apply nonlinear elements to different geometric load patches to capture the energy dissipation at a joint interface.

6.1 Linear Reduction – Coppolino Method

The second reduction technique evaluated was Coppolino Reduction. For this reduction, the interface was segmented into the following load patches: (1) one load patch that maintains all the DOF of each interface, and (2) two load patches that divide the DOF to two separate interfaces. It is important to consider the rotational rigid body modes when obtaining the basis for the reduction; the frequency errors without these is substantial. Table 5 shows the frequency error for Coppolino reduction when one and two load patches are used to reduce the interface for each end of the S4 beam.

Table 5: Frequency error for the first six modes with one load patch vs. two load patches for Coppolino reduction

Mode	HCB Model Frequency (Hz)	1 Load Patch Coppolino Model Frequency Error	2 Load Patch Coppolino Model Frequency Error
1	132.83	3.08%	1.33%
2	249.15	12.74%	5.17%
3	275.02	4.68%	4.56%
4	317.83	4.19%	1.19%
5	384.89	57.39%	48.76%
6	578.39	36.62%	8.51%

Joining the whole interface in a single load patch was found to give substantial frequency errors for modes 2, 5, and 6, indicating an overly stiff interface. When the interface was divided into two load patches reduces the frequency error of most modes to below 10% with the exception of mode 5. The MAC between the Coppolino reduced modes and the HCB reduced modes gives further insight into the effectiveness of this reduction technique and is shown in Figure 12.

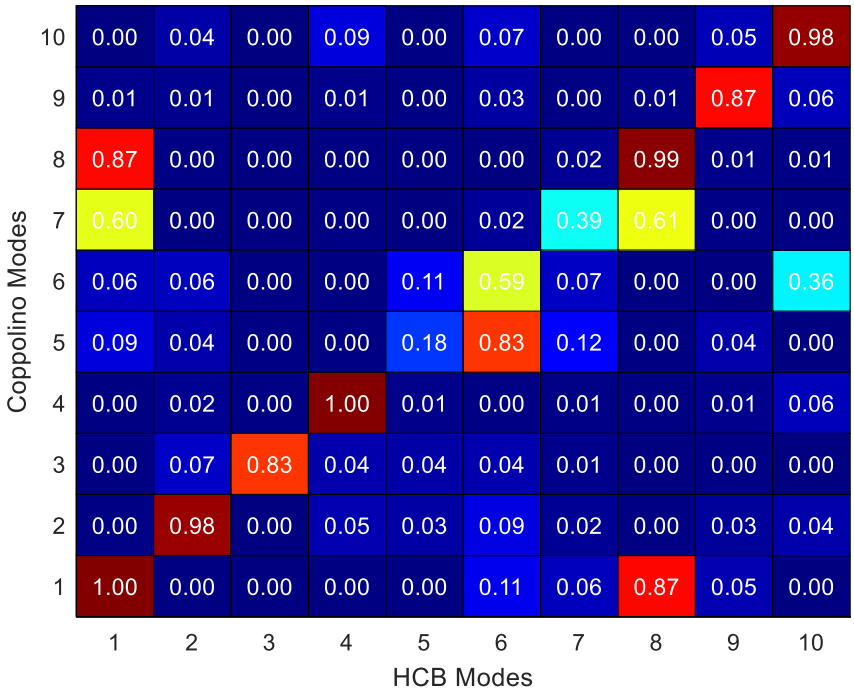

Figure 12: Visual representation of the MAC between the Coppolino reduced modes and the HCB reduced modes

With the exception of modes 5-7, there is good correlation between the modes of the HCB model and the Coppolino reduced model. Furthermore, the Coppolino reduced model captures the higher order modes (8-10) better than the S-CC reduced model. Table 6 shows a summary of the frequency errors relative to the HCB model for the S-CC Reduction with 6 constraint modes and the Coppolino Reduction with two load patches for the fully stuck case. The respective sizes of the mass and stiffness matrices

including 20 fixed interface modes is $[3614 \times 3614]$ for HCB, $[26 \times 26]$ for S-CC, and $[32 \times 32]$ for Coppolino.

Table 6: Frequency error comparison for the first six modes for the HCB model versus the S-CC reduced model with 6 shapes and the Coppolino reduced model with 2 load patches for the fully stuck case

Mode	HCB Model Frequency (Hz)	6 S-CC Shape Reduction Model Frequency Error	2 Load Patches Coppolino Model Frequency Error
1	132.83	0.0005%	1.33%
2	249.15	0.0002%	5.17%
3	275.02	0.003%	4.56%
4	317.83	0.02%	1.19%
5	384.89	0.013%	48.76%
6	578.39	0.28%	8.51%

Although the frequency errors are not below 1%, the Coppolino reduction technique is expected to have certain merits when it comes to nonlinear characterization. Each load patch can have a different stiffness and different nonlinear joint, and as a result this might capture different behaviors of the interface such as no contact, microslip, and macroslip. Furthermore, the Coppolino method contains shapes that are dominated by axial motion of the interfaces, something that is missed by the S-CC basis.